FUSIONAL METHOD OF MPS AND FEM THROUGH TETRAHEDRAL MESH GENERATION

JUNYA IMAMURA[1]

[1]*imi* Computational Engineering Laboratory
Wako-shi, Honcho 31-9-803, 351-0114 Saitama, Japan
E-mail: jimamura@ra2.so-net.ne.jp

Key words: Improved Helmholtz-decomposition, MPS, FEM, Non-equidistant FDM

Abstract. The moving-particle semi-implicit (MPS) method is used as a density method for moving surfaces. The main disadvantage of previous density methods was that mass conservation was difficult to achieve because the mean density varied due to elemental diffusion; in contrast, MPS satisfies mass conservation. The density method is also very suitable as a finite element method (FEM), thus leading to the concept of an MPS-FEM fusion method. The MPS method especially incorporates a weight function for calculating the particle number density. Because the weight function is a Kernel function, the MPS-FEM fusion method includes a novel Kernel function similar to the weight function of MPS. The masses (particles) occupy positions on the vertex nodes of the tetrahedral elements, and the mesh must be recomposed for the time step advance by using a mesh generation technique. The masses are distributed in the control volume (CV) according to the Karnel function, and mass conservation must be satisfied by mesh regeneration using the apparent new density ρ. The method is composed of FEM and a conceptual Helmholtz decomposition (*H-d*) using $\boldsymbol{u}^L$- and $\boldsymbol{u}^T$-elements for displacement $\boldsymbol{u} = \boldsymbol{u}^L + \boldsymbol{u}^T$ (where *L*: *Lateral* and *T*: *Transverse*). Nevertheless, an improved Helmholtz decomposition method (*iH-d*) is applied here to satisfy the conservation laws.

1 INTRODUCTION

I present a numerical calculation model of an incompressible flow field with free surfaces. The model is based primarily on the moving-particle semi-implicit (MPS) method, but calculation is performed by the finite element method (FEM) to include not only scalar potential flow but also vorticity flow. Thus, I apply Helmholtz decomposition (*H-d*) to represent the velocities.

Moreover, I consider the scalar potential term of *H-d* inappropriate to represent dilatational components. For this reason, I propose an improved Helmholtz decomposition (*iH-d*). The objective of the present study is to build a route for applying *iH-d* to free surface flow problems.

MPS is the best method for such free surface problems, because it conserves mass perfectly and is the only method disregarding surfaces. In addition, MPS allows nonlinear mechanisms, and it can therefore be used to solve contact problems. In the flow problem, the free surface implies mechanism nonlinearity, i.e., changes from the Dirichlet boundaries to the Neumann boundaries or the reverse.

In the free-surface MPS problem, the compressible flow plays an important role because this is apparently a compressible flow problem. Therefore, FEM is required for the compressible

flow calcuation.

The *iH-d* method allows compressibility by representing the velocity vector separately, i.e., with the dilatational term and the rotational term.

The *iH-d* rotational term is incompressible at any time (automatically solenoidal). However, not only vorticity but also the shear strains in the fluid must be incompressible.

Normal strains induce volume changes, whereas shear strains induce shape changes but no volume changes. This is the basic assumption for applying *iH-d* to free-surface problems.

In reverse, MPS causes high discretization (example discretization model shown in Fig. 1).

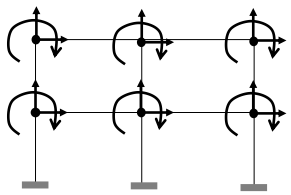

Figure 1: Nodal model (continua → Frame work)

This problem can be explained by Kondo's indication [3] that the original MPS formulation lacks angular momentum terms. For the equilibrium equations of the above framework model, $\Sigma M_i=0$ is required in addition to $\Sigma N_i=0$ on the nodes. This problem is automatically resolved when we use FEM, in which distributed rigidity and re-reduced particle density is assumed.

2 REDUCING AND RE-REDUCING: FINITE ELEMENTS ←→ PARTICLES

2.1 Initial setting

The numerical scheme is constructed by FEM, generating tetrahedral elements by joining two particles with a straight line. This process is called grid generation in initial setting.

The particles include inner mass particles and boundary particles, and the boundary particles include zero-mass particles on the Dirichlet boundary and nonzero–mass particles on the Neumann boundary; nonequal masses are allowed.

At the time of the initial setting, the system is divided into sub-domains, and all particles are set on the centre of gravity, with the exception of the particles on the Neumann boundary. Overall, the following steps are executed:

(1) Setting the nodes on the Dirichlet boundaries → without mass (zero-mass)
(2) Setting the nodes on the Neumann boundaries → with mass
(3) Dividing the system to sub-domains for particles with mass → infinite number and mass
(4) Constructing the tetrahedral elements (by any existent scheme) → nonequally masses are allowed
(5) Adaptive element generation for isolated (flying) particles (in future work)

The above steps are illustrated in Fig. 2.

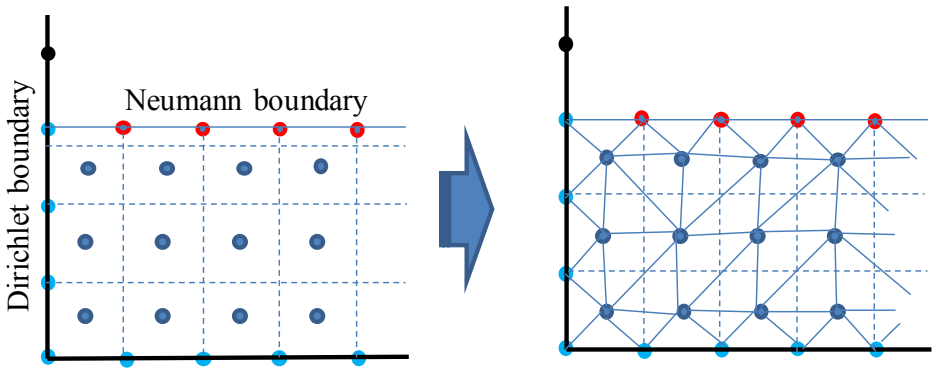

Figure 2: Initial setting procedure

2.2 Re-reducing particle mass to density

To apply FEM, density is indispensable. m_i is the mass of the concerned particle i, $V_{j,i}$ is the control volume (CV) of the j-th element that shares a node with i, and the mass m_i is distributed to the individual CV in the inverse ratio following Eq. (1).

$$\frac{1}{V_{i,1}} : \frac{1}{V_{i,2}} : \frac{1}{V_{i,3}} : \cdots : \frac{1}{V_{i,n}} \tag{1}$$

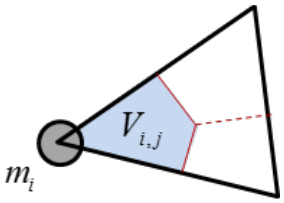

Figure 3: Re-reducing of particle mass to ρ

ρ has a positive physical value, so it is represented by the exponent of the r-variable, i.e., $\rho = exp(r)$. ρ is constant in CV, but discontinuous in the element; consequently, mass conservation is shown in (2) without advection terms.

$$\frac{D\rho}{Dt} + \rho div\boldsymbol{U} = 0 \;\rightarrow\; \frac{\partial r}{\partial t} + div\boldsymbol{U} = 0 \tag{2}$$

3 IMPROVED HELMHOLTZ DECOMPOSITION

3.1 Helmholtz decomposition

According to the Helmholtz theorem, an arbitrary vector field $\boldsymbol{u}$ can be represented in Eq. (3) using a scalar potential $\nabla\phi$ and a vector potential $\boldsymbol{\psi}$ under the restriction of the Coulomb gauge.

$$\boldsymbol{u} = \nabla\phi + curl\boldsymbol{\psi} \quad (div\boldsymbol{\psi} = 0) \tag{3}$$

Let us think about the displacement vector $\boldsymbol{u}$ in a solid. The simplest example is the cantilever, which is statically deterministic and can neglect the shearing strain, i.e., $\boldsymbol{u}=\nabla\phi$.

However, we cannot obtain the numerical result expected by FEM using $\nabla\phi$.

3.2 Improved Helmholtz decomposition

Therefore, I proposed the improved Helmholtz decomposition represented in Eq. (4).

$$\left.\begin{array}{l} \text{fluid} : \boldsymbol{u} = (\nabla_{diag}\boldsymbol{\psi} + \nabla\phi) + \nabla_{curl}\boldsymbol{\psi} \\ \text{solid} : \boldsymbol{u} = (\nabla_{diag}\boldsymbol{\psi} + \nabla\phi) + \nabla_{shr}\boldsymbol{\psi} \end{array}\right\} \quad (\nabla\phi \Rightarrow \boldsymbol{0}, div\nabla_{shr}\boldsymbol{\psi} = 0) \quad (\Rightarrow 0 \quad \text{means minimize}) \tag{4}$$

The novel operator used in Eq. (4) is defined as follows:

$$\text{Def. of novel operator}: \begin{Bmatrix} \nabla_{diag} \\ \nabla_{shr} \\ \nabla_{curl} \end{Bmatrix} \boldsymbol{u} \equiv \begin{Bmatrix} \boldsymbol{\varepsilon} \\ \boldsymbol{\gamma} \\ \boldsymbol{\omega} \end{Bmatrix}, \qquad where \quad 2\nabla\boldsymbol{u} = \begin{bmatrix} \varepsilon_1, & \gamma_3, & \gamma_2 \\ \gamma_3, & \varepsilon_2, & \gamma_1 \\ \gamma_2, & \gamma_1, & \varepsilon_3 \end{bmatrix} + \begin{bmatrix} \varepsilon_1, & -\omega_3, & \omega_2 \\ \omega_3, & \varepsilon_2, & -\omega_1 \\ -\omega_2, & \omega_1, & \varepsilon_3 \end{bmatrix}, \quad \gamma_i \equiv \gamma_{i-1,i+1}$$

$$(i = 1,2,3)(i+1 = 2,3,1)(i-1 = 3,1,2)$$

$$(\therefore i+2 = i-1, \; i-2 = i+1)$$

$$\begin{Bmatrix} \nabla^2_{diag} \\ \nabla^2_{shr} \\ \nabla^2_{curl} \end{Bmatrix} \equiv \begin{Bmatrix} \nabla_{diag}\nabla_{diag} \\ \nabla_{shr}\nabla_{shr} \\ \nabla_{curl}\nabla_{curl} \end{Bmatrix}$$

The expression for the fluid in the definition assumes that the Navier–Stokes (N.S.) equation is represented in rotational form. When the N.S. equation is represented in shearing form, the expression in the second row (using $\nabla_{shr}\boldsymbol{\psi}$) is the same as for the solid.

The dilatational component in *iH-d* is represented by the orthogonal component of the rotational components and modified with $\nabla\phi$, which is constrained by the gauge.

3.3 Strain potential and chain low

According to the Helmholtz theorem, the arbitrary vector field should be decomposed. By analogy to the numerical formula, *iH-d* can be applied to the strain vector shown in Eq. (5).

$$\text{"}strain\ \ potential\text{"}: \quad \left.\begin{array}{l} \boldsymbol{\omega} = (\nabla_{diag}\boldsymbol{\Psi} + \nabla\Phi) + \nabla_{curl}\boldsymbol{\Psi} \\ \boldsymbol{\gamma} = (\nabla_{diag}\boldsymbol{\Psi} + \nabla\Phi) + \nabla_{shr}\boldsymbol{\Psi} \end{array}\right\} \quad (\nabla\Phi \Rightarrow \boldsymbol{0}, div\nabla_{shr}\boldsymbol{\Psi} = 0) \tag{5}$$

$$where \quad \begin{cases} \boldsymbol{\omega} \equiv \{\varepsilon_i\} + \{\omega_i\} \\ \boldsymbol{\gamma} \equiv \{\varepsilon_i\} + \{\gamma_i\} \end{cases}$$

iH-d decomposes also the vector potential $\boldsymbol{\psi}$ shown in Eq. (6).

$$\boldsymbol{\psi} = (\nabla_{diag}\boldsymbol{\psi} + \nabla\vartheta) + \nabla_{curl}\boldsymbol{\psi} \quad (\nabla\vartheta \Rightarrow 0, \; div\nabla_{curl}\boldsymbol{\psi} = 0) \tag{6}$$

I call the above the “low chain of the Helmholtz decomposition”. The low chain can be endlessly developed, and, therefore, *iH-d* can only be represented numerically.

3.4 Scoop up residuals of an equation to $\nabla\phi$

The scalar potential ϕ and the pressure P function have the same spatial effects. The dilatational component modified by $\nabla\phi$, $\nabla_{diag}\boldsymbol{\psi}$, represents the volumetric ratio $div\boldsymbol{u}^L=div\nabla_{diag}\boldsymbol{\psi}$. The conceptual function of $\nabla\phi$ is illustrated in Fig. 4. The numerical scheme for minimizing ($\nabla\phi\Rightarrow\boldsymbol{0}$) consists of two steps. First, $\nabla\phi$ scoops up the residual of an equation represented by $\boldsymbol{u}$, e.g., $A+div\boldsymbol{u}^L \rightarrow \nabla\phi$(Eq. (7)), and then $\nabla\phi$ gives the offset values of $\boldsymbol{u}$ which are explained later (in the section 4.7).

$$\int_{\Omega}\{(A+divu)+\nabla\phi\}\cdot\delta\nabla\phi d\Omega=0 \tag{7}$$

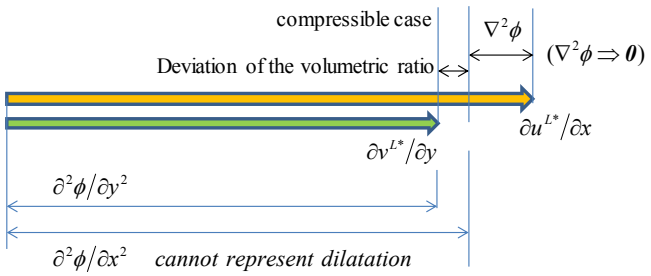

Figure 4: Conceptual function of $\nabla\phi$

3.5 *iH-d* elements

I propose the *iH-d* elements in Fig. 5, in which shows an example of $\nabla\phi$. This element shape is applied for $\nabla\psi_i$, $\nabla\Phi$, nd ∇P. ({ }$_k$: on vertex, { }$_{COG}$: on the center of gravity)

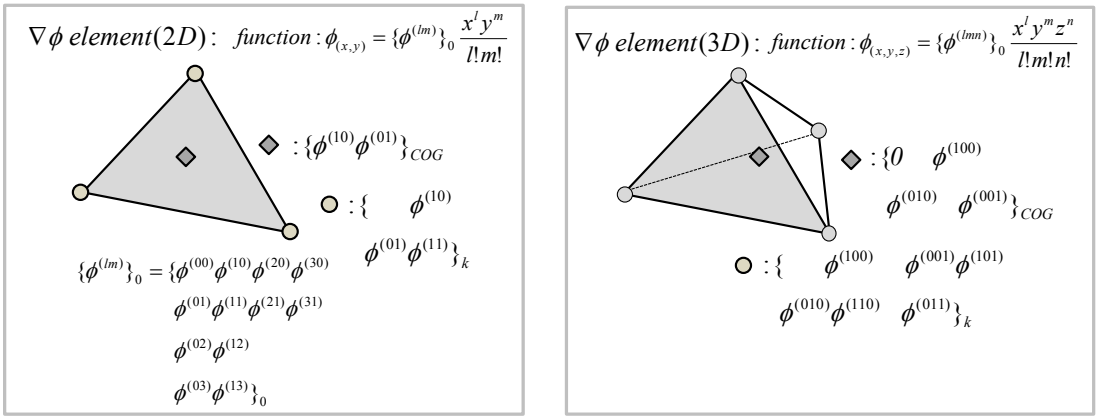

Figure 5: *iH-d* elements $\nabla\phi$ for 2D and 3D

The element function is expressed in the finite Taylor series, and the adopted terms are represented in Fig. 5 with the coefficient terms for 2D in the left part of the figure (no notice for 3D). The functions for 2D and 3D are incomplete 3rd order functions. Both functions have a zero interceptor $\{\phi^{(00)}\}_0=0$.

4 NUMERICAL SCHEME

4.1 Navier–Stokes equation

The mass conservation equation is shown in Eq. (2). The Navier–Stokes equation used in this paper is shown in Eq. (8) in the rotational form, where $\boldsymbol{U}$ is the velocity vector, ρ is the density, $\boldsymbol{g}$ is the gravity, P is the pressure, and μ is the viscosity.

$$\rho\left(\frac{D\boldsymbol{U}}{Dt}+\boldsymbol{U}\cdot div\boldsymbol{U}-\boldsymbol{g}\right)+\nabla P-\mu\left(\frac{4}{3}\nabla div\boldsymbol{U}-\nabla^2_{curl}\boldsymbol{U}\right)=0 \tag{8}$$

4.2 Time axially central FDM

I apply the central difference method to the time axis shown in Eq. (9), where $\boldsymbol{u}$ is the displacement vector, Δt is the time pitch, and n is the time step ($n=0,1,2,3,\cdots$).

$$U_i^n=\frac{u_i^{n+1}-u_i^{n-1}}{2\Delta t},\quad \left\{\frac{\partial U_i}{\partial t}\right\}^n=\frac{u_i^{n+1}-2u_i^n+u_i^{n-1}}{\Delta t^2} \tag{9}$$

The states are known for *n-1* and *n* , and unknown for *n-1*, and the displacements $\boldsymbol{u}^{L,n+1}$ and $\boldsymbol{u}^{T,n+1}$ are used as variables, i.e., unknown parameters $\{\nabla\boldsymbol{\psi}\}_k^{n+1}$, $\{\nabla\boldsymbol{\psi}\}_{COG}^{n+1}$

ρ, $\nabla\phi$, $\nabla\Phi$, and ∇P are the elements used here.

For *n-1* and *n+1*, I use the grid generated at *n*, but using the corresponding data for each spatial position shown in Fig. 6

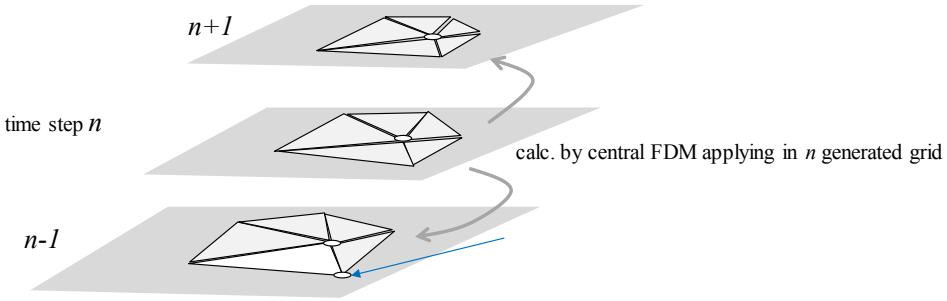

Figure 6 Grid usage

4.3 Initial setting of ∇P element

The gravity acceleration g_z and the density ρ_0 are known, and so the node parameter $\{P^{(001)}\}_k$ can be determined algebraically, using Eq. (10).

$$\{P^{(001)}\}_k=\rho_0 g_z \tag{10}$$

By this initial setting, the system is maintained stable, and ∇P triggers the dam breaking problem, as is shown for example in Fig. 7.

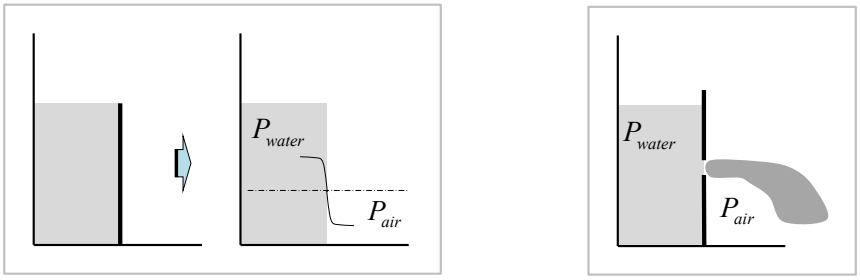

Figure 7 Dam breaking and discharge

4.4 Momentum conservation excluding source and charge

The Navier–Stokes equation is resolved on the time step *n*-section by iteration, through the weighted residual method.

The scheme can be explained better by dividing it into step groups. In the first step group, elements $\nabla\phi$, ρ, ∇P, $\nabla\Phi$ are calculated, and in the second step group, element $\nabla\boldsymbol{\psi}$ is calculated.

The concept of the proposed scheme is explained by Eq. (11) and Eq. (12), where $\boldsymbol{1}\equiv\{1,1,1\}$.

$$\frac{\partial\rho}{\partial t}+\boldsymbol{U}\cdot\nabla\rho+\rho(div\boldsymbol{U}^{L}+\nabla^{2}\phi)=0 \tag{11}$$

$$\{\rho(\frac{\partial\boldsymbol{U}}{\partial t}+\boldsymbol{U}\cdot\nabla\boldsymbol{U}-\boldsymbol{g})+\rho_{0}\boldsymbol{g}+\nabla P\}-\mu\{\frac{4}{3}\nabla(div\boldsymbol{U}^{L}+\boldsymbol{1}\cdot\nabla\Phi)-\nabla^{2}_{curl}\boldsymbol{U}^{T}\}=0 \tag{12}$$

Both equations mean to conserve the momentum excluding sourcing and charging into the system.

Eq. (11) excludes sourcing through a continuity equation using $\nabla\phi$.

Eq. (12) excludes external force sourcing using ∇P and internal force sourcing using $\nabla\Phi$. The solenoidal term is unrelated to sourcing.

4.5 Boundary value problems for *iH-d* elements

The *iH-d* element satisfies C^{1}-continuity. However, the boundary value problem is incompatible with C^{1}-continuity, because up to 2nd derivative must be determined with other conditions explained in Eq. (13), or by the hybridization method shown in Eq. (14).

$$\beta u+\alpha\frac{\partial u}{\partial n}\ \Big|\ \frac{\partial^{2}u}{\partial n^{2}},\frac{\partial^{2}u}{\partial s\partial n},\cdots\ \Rightarrow to\ be\ solved\ by\ other\ condition \tag{13}$$

$$\left.\begin{aligned}\beta\theta+\alpha\frac{\partial\theta}{\partial n}=\varphi\quad on\Gamma\quad(\nabla\phi-\theta\Rightarrow 0\quad in\Omega)\\ \beta\Lambda+\alpha\frac{\partial\Lambda}{\partial n}=\vartheta\quad on\Gamma\quad(\nabla\theta-\Lambda\Rightarrow 0\quad in\Omega)\end{aligned}\right\} \tag{14}$$

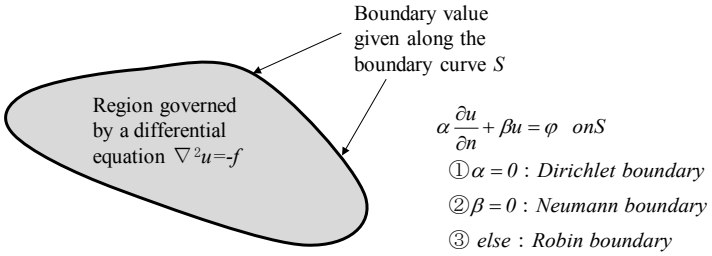

Figure 8 The boundary value problem

Thus (according to the former), the twist parameter is varied on the vertex in order to minimize the twist value in the element shown in Eq. (15) ($\{\phi^{(11)}\}_k$: free on the boundary).

$$\int_{\Omega} \phi^{(11)} \cdot \frac{\partial \phi^{(11)}}{\partial \{\phi^{(11)}\}_k} d\Omega = 0 \tag{15}$$

Eq. (15) is represented in the 2D case. Up to the 2nd derivative can be varied, but the constraint condition is represented as ($\phi^{(11)} \Rightarrow 0$) for simplicity.

4.6 The first group step

The node parameters $\{\nabla \phi\}_k$, ρ, $\{\nabla P\}_k$ and $\{\nabla \Phi\}_k$ are obtained from Eq. (16).

$$\left.\begin{aligned}
&① \ \nabla\phi \leftarrow \int_{\Omega} \{(\frac{\partial r}{\partial t} + div\boldsymbol{U}^L)\cdot \boldsymbol{I}^T + \nabla^2_{diag}\phi\}\cdot\delta\nabla^2_{diag}\phi\}d\Omega = 0 \quad (\phi^{(11)} \Rightarrow 0)\\
&② \ \rho : r \leftarrow \int_{CV} \{\frac{\partial r}{\partial t} + div(\boldsymbol{U}^L + \nabla\phi)\}\cdot\delta r\}d\Omega = 0 \quad inCV\\
&③ \ \nabla P \leftarrow \int_{\Omega} \{\rho(\frac{D\boldsymbol{U}^L}{Dt} - \boldsymbol{g}) + \rho_0\boldsymbol{g} + \nabla P\}\cdot\delta\nabla P\}d\Omega = 0 \quad (P^{(11)} \Rightarrow 0)\\
&④ \ \nabla\Phi \leftarrow \int_{\Omega} \{(div\boldsymbol{u}^L\cdot\boldsymbol{I}^T + \nabla\Phi)\}\cdot\delta\nabla\Phi\}d\Omega = 0 \quad (\Phi^{(11)} \Rightarrow 0)
\end{aligned}\right\} \tag{16}$$

4.7 The second step

The node parameters $\{\nabla \boldsymbol{\psi}\}_k$ are obtained from Eq. (17) and the accompanying constraint condition is shown in the 2nd row.

The incremental $\{\nabla \Delta\boldsymbol{\psi}\}_k$: $\Delta\boldsymbol{U}$ are unknown parameters in the simultaneous equation.

$$\begin{aligned}
⑤ \ \nabla\boldsymbol{\psi} \leftarrow & \int_{\Omega} \{\rho(\frac{D\boldsymbol{U}}{Dt} - \boldsymbol{g}) + \rho_0\boldsymbol{g} + \nabla P - \mu(\frac{4}{3}\nabla div\boldsymbol{U}^L - \nabla^2_{curl}\boldsymbol{U}^T)\}\cdot\delta\nabla\boldsymbol{\psi}\ d\Omega\\
& + \int_{\Omega} \{\frac{1}{\Delta t}(\Delta\boldsymbol{U}^L - \nabla\phi) + \nu\frac{4}{3}(\nabla_{diag}\Delta\boldsymbol{U}^L - \nabla\Phi)\}\cdot\delta\nabla\boldsymbol{\psi}\ d\Omega = 0 \quad (\psi_i^{(11)} \Rightarrow 0)
\end{aligned} \tag{17}$$

$$where\ \boldsymbol{U}^m = \boldsymbol{U}^{m-1} + \Delta\boldsymbol{U} \quad (m = 0,1,2,3,\cdots)$$

①～⑤ are iterated until converged.

4.8 Gauge for *iH-d* scheme

$\nabla \boldsymbol{\psi}$ have ninedegrees of freedom. Therefore, nine equations are needed to obtain *iH-d* parameters. (Notice; Using the cubic interpolation procedure (CIP), ∇(N.S. eq.) = *0* is solved to obtain $\nabla \boldsymbol{u}$.)

I call the relationship between $\nabla_{curl}\boldsymbol{\psi}$ and $\nabla_{shr}\boldsymbol{\psi}$ "conjugate". $\nabla_{curl}\boldsymbol{\psi}$ is a conjugate variable of $\nabla_{shr}\boldsymbol{\psi}$ and vice versa.

The Eq. (9) supplement constraint condition ($\nabla_{shr}\boldsymbol{\psi} \Rightarrow \boldsymbol{0}$) stabilizes the numerical calculation. I call this conditions also "gauge".

To calculate $div\boldsymbol{u}$, a gauge ($\nabla_{imi}\boldsymbol{u} \Rightarrow \boldsymbol{0}$) is necessary, as seen in Eq. (18) and Eq. (19); a novel operator ∇_{imi} is defined in Eq. (19).

$$2div\boldsymbol{u} = 2(\frac{\partial u}{\partial x}+\frac{\partial v}{\partial y}+\frac{\partial w}{\partial z}) = (\frac{\partial u}{\partial x}+\frac{\partial v}{\partial y})+(\frac{\partial v}{\partial y}+\frac{\partial w}{\partial z})+(\frac{\partial w}{\partial z}+\frac{\partial u}{\partial x}) \tag{18}$$

$$\boldsymbol{1}\cdot\nabla_{imi}\boldsymbol{u} \equiv (\frac{\partial u}{\partial x}-\frac{\partial v}{\partial y})+(\frac{\partial v}{\partial y}-\frac{\partial w}{\partial z})+(\frac{\partial w}{\partial z}-\frac{\partial u}{\partial x}) \tag{19}$$

5 PARTICULARITY OF 2D MODEL

To ensure the above 2D scheme is necessary condition to ensure the 3D calculations.

The Helmholtz decomposition (Eq. (3)) for < x−y > 2D can be represented in Eq. (20) using the suffices (*i = 1, 2, 3*), (*i + 1 = 2, 3, 4*), and (*i−1 = 3, 1, 2*); also, for < y−z > 2D it is shown in Eq. (21).

$$<x-y>2D\begin{cases} u=\dfrac{\partial\phi}{\partial x}+\dfrac{\partial\psi_3}{\partial y} \\ v=\dfrac{\partial\phi}{\partial y}-\dfrac{\partial\psi_3}{\partial x} \end{cases} \Rightarrow \begin{cases} u_i = \dfrac{\partial\phi}{\partial x_i}+\dfrac{\partial\psi_{i-1}}{\partial x_{i+1}} \\ u_{i+1}=\dfrac{\partial\phi}{\partial x_{i+1}}-\dfrac{\partial\psi_{i-1}}{\partial x_i} \end{cases} \tag{20}$$

$$\Downarrow$$

$$<y-z>2D\begin{cases} v=\dfrac{\partial\phi}{\partial y}+\dfrac{\partial\psi_1}{\partial y} \\ w=\dfrac{\partial\phi}{\partial z}-\dfrac{\partial\psi_1}{\partial y} \end{cases} \Leftarrow \begin{cases} u_{i+1} = \dfrac{\partial\phi}{\partial x_{i+1}}+\dfrac{\partial\psi_i}{\partial x_{i+2}} \\ u_{i+2}=\dfrac{\partial\phi}{\partial x_{i+2}}-\dfrac{\partial\psi_i}{\partial x_{i+1}} \end{cases} \tag{21}$$

We can express it in the same way also for < z−x > 2D. 3D can be expressed by summation of these equations. Thus, it is sufficient by the explanation for 2D.

However, in 2D, $\nabla_{diag}\boldsymbol{\psi}$ cannot be applied, because ψ_1 and ψ_2 are lacking in $\nabla_{curl}\boldsymbol{\psi}$.

It must be remembered that the 2D model calculates 3D, and the axisymmetric 1D model do also 3D.

Accordingly, the 2D model can be used to represent 3D by introducing the *z*-axis shown in Eq. (22).

$$\left.\begin{aligned}\psi_1 &= g_{1,(x,y)} + z \cdot g_{2,(x,y)} \\ \psi_2 &= h_{1,(x,y)} + z \cdot h_{2,(x,y)}\end{aligned}\right\} \tag{22}$$

Nevertheless, it must also be remembered that the integrals of the odd functions $z \cdot g_2$' are zeros.

The vertex stretching terms also appear by introducing the *z*-axis; theoretically, these stretching terms are zeros in 2D. This means that the *iH-d* scheme using Eq. (22) satisfies [stretching terms=***0***], numerically.

6 CONCLUSIONS AND FUTURE WORKS

- The biggest merits of MPS are that it conserves mass perfectly, and is not affected by the existence of surfaces. Conversely, these are the week points of FEM.
- One of the characteristics of FEM is that it can be used for calculations without angular momentum terms.
- I proposed in this paper an MPS-FEM fusion method that incorporates the advantages of both models.
- I interpret MPS as a sort of density method for a moving surface.
- Accordingly, the fusion method may be used for compressible flow calculations.
- I apply here the *iH-d* elements and scheme.
- Going further, in my future work, I am going to finish developing an adoptive scheme for maintaining a tetrahedral element by sub-division of a particle.
- The numerical verifications are also going to be conducted in the near future.
- The forced cavity must be chosen as a benchmark test problem to verify the results of this paper.

REFERENCES

[1] K. Sugihara and J. Imamura, *Stress analysis by non-equidistant finite difference method (4th paper)*, Transaction of AIJ, vol.178, pp. 17-24, (1970).
[2] J. Imamura and T. Tanahashi, *Improved HSMAC method: An improvement based on Helmholtz-Hodge theorem*, Transaction of JSCES, Paper No. 20100010, (2010).
[3] M. Kondo, *Angular momentum conserving particle method for high viscos fluid calculation*, Proceedings of the conference on computational engineering and science, vol. 22, JSCES, 2017
[4] J. Imamura, *Proposal of improved Helmholtz-decomposition and the finite element, and application to fluid and solid*, vol. 22, JSCES, 2017
[5] J. Imamura, *Helmholtz-decomposition of solid, and study on Eulerian solution*, vol. 22, JSCES, 2017
[6] J. Imamura, *Concept of fusional method of MPS and FEM through non-equidistant finite difference method*, vol. 22, JSCES, 2017
[7] A.E.H. Love, *A treatise on the mathematical theory of elasticity*, Dover Publications, 1926
[8] Y.C. Fung, *Foundation of solid mechanics*, Prentice-Hall, 1965